Atmos. Chem. Phys. Discuss., 12, 10623–10649, 2012
www.atmos-chem-phys-discuss.net/12/10623/2012/
doi:10.5194/acpd-12-10623-2012

Atmospheric Chemistry and Physics Discussions

Anthropogenic CO_2 flux constraints in the Tokyo Bay Area from Lagrangian diffusive backward trajectories and high resolution in situ measurements

I. Pisso[1], P. Patra[1], M. Takigawa[1], T. Machida[2], H. Matsueda[3], and Y. Sawa[3]

[1]Research Institute for Global Change, JAMSTEC, Yokohama 236 0001, Japan
[2]National Institute for Environmental Studies, Tsukuba, Ibaraki 305-8506, Japan
[3]Meteorological Research Institute, Tsukuba, Ibaraki, 305-0052 Japan

Received: 26 March 2012 – Accepted: 4 April 2012 – Published: 24 April 2012

Correspondence to: I. Pisso (ignacio@jamstec.go.jp)

Published by Copernicus Publications on behalf of the European Geosciences Union.

Abstract

In order to use high resolution in-situ measurements to constrain regional emissions of carbon dioxide (CO_2), we use a Lagrangian methodology based on diffusive backward trajectory tracer reconstructions. We use aircraft, tall tower and ground sites for CO_2 data collected nearby the CO_2 emission hot spot of the Tokyo Bay Area during the CONTRAIL campaign, from the MRI/JMA Tsukuba tall tower and from the World Data Centre for Greenhouse Gases (WDCGG). We calculated Bayesian inversions based on EDGAR 4 and CDIAC a priori fluxes. Estimated fluxes for the Tokyo Bay Area for the analyzed period between 2005 and 2009 range between 4.80×10^{-7} and $3.45 \times 10^{-6}\,kg_{CO_2}\,m^2\,s^{-1}$ with significant time variations. Significant differences in retrieved fluxes of up to 21 % were found when CONTRAIL measurements were added to the dataset. No significant trend was found in the time series of spatially averaged retrieved fluxes.

1 Introduction

Anthropogenic emissions of CO_2 and in general greenhouse gases (GHGs) are a major concern for atmospheric composition, given that emissions are increasing rapidly with a consequent impact on the atmospheric radiative budget. Estimations of CO_2 fluxes at continental scales contain significant uncertainties, and these uncertainties are larger for finer spatial and temporal scales. Such uncertainty limits the rapid development of comprehensive mitigation policies at global and State levels. In the so called "bottom-up" approach, CO_2 emissions from fossil fuel consumption are estimated based on socio-economic databases (European Comission, 2009). Their accuracy depends on the reliability of information about the import, export and consumption of fossil fuels by various countries. Therefore, complementary independent assessment is desirable.

The atmospheric CO_2 measurements record the effect of CO_2 surface sources on the earth's atmospheric composition. Consequently, time series of atmospheric CO_2 con-

ACPD
12, 10623–10649, 2012

centrations and transport model simulations can be used for constraining the surface fluxes by the so called top-down approach or inverse modeling. In the inverse approach, for any given atmospheric transport model, it is theoretically possible to linearize and invert the transport operator in order to relate perturbations to the background (e.g. anthropogenic emissions) with a measured concentration. ($\Delta F = \Delta\chi_{CO_2} \frac{\partial F}{\partial \chi_{CO_2}}$ where F is the flux, χ is the mixing ratio and $\frac{\partial \chi_{CO_2}}{\partial F}$ the linearized transport operator.) The other approach consists of local micro-scale flux measurements (Moriwaki and Kanda, 2004), which are suitable for small patches (a few 100 m^2), but it is not feasible for monitoring an area of the size of the Tokyo Bay Area.

Nevertheless, in real world applications the amount of information available is seldom sufficient, and hence this formulation yields ill-conditioned problems, that are challenging to solve numerically. A number of regularization mechanisms have been proposed and applied to the important problem of constraining global biogenic inversions (e.g., Enting, 2002; Tarantola, 2005).

Regional (10^4 km^2) assessments of fluxes using global models are hindered at small time and space scales due to models inability to represent CO_2 time series measurements adjacent to large point sources (Patra et al., 2008). A more precise methodology is desirable, as errors can amount to 200 % in regional flux estimation from global Eulerian models (Gurney et al., 2002). Mesoscale CO_2 flux inversion is gaining popularity in both Eulerian and Lagrangian modeling research. A number of previous studies have focused on biogenic emissions. Lin et al. (2007) based on the model STILT, provided flux estimates based on footprint analysis. Tolk et al. (2009) analized the Cabauw tower data using a mesoscale model. Lagrangian inversion has been recently used in the lower troposphere close to the surface to estimate biogenic emissions (Lauvaux et al., 2009). The specific problem of anthropogenic emissions requires spatial scales the size of a city in order to be resolved, and hence Lagrangian-based techniques are well suited for this application. The Tokyo Bay Area (TBA) is among the largest emission spots on the surface of the Earth, a highly developed area with nearly 30 million inhabitants, a significant industrial activity and a complex transportation network. It is

ACPD
12, 10623–10649, 2012

located in a terrain with varied topography and surrounded by a complex coast line in the East.

In this study we estimate CO_2 flux constraints based on Lagrangian backward transport modeling and an inverse Bayesian methodology. We present a case study of the TBA using ensembles of diffusive backward trajectories (Pisso et al., 2010) and a Lagrangian particle dispersion model de Foy et al. (2009, FLEXPART-WRF) with different advecting winds, parametrizations of turbulent mixing and simplified planetary boundary layer (PBL) interface representations. The fluxes were calculated for the winter months (December to March) when the inventories show that biospheric activity within the TBA can be considered to have a lesser impact on CO_2 concentrations than anthropogenic activity. This study, to our knowledge the first of its kind in Japan, is organized as follows: Sect. 2 introduces the models, methods and data used in this study, Sect. 3 describes the results obtained, Sect. 4 discusses these results and Sect. 5 presents our conclusions.

2 Method

In order to constrain emission fluxes with concentration or mixing ratio measurements far away from the CO_2 source, the transport and mixing processes determining the impact of the source on the receptor must be assessed. Given certain information about the transport and mixing, the master equation $G_{i,j} = P(i \rightarrow j)$ allows us to extract the source distributions (initial/boundary conditions) that best represent the tracer measurements according to certain criteria (Risken, 1989). $G_{i,j}$ describes the probability of a transition between the location i to the location j. Atmospheric transport and mixing models (particularly Lagrangian) are often applied to the numerical representation of the transition probability or master equation. Because the Green's function discretization is only suitable for concentrations or mixing ratios, the 2-D to 3-D conversion from flux to volume has to be calculated. Source Relation Relationships (SRRs) (Seibert and Frank, 2004) were developed to assess the probability that a receptor (e.g., an

ACPD
12, 10623–10649, 2012

atmospheric measurement site) is linked with a source depending on the time a back trajectory spends in a grid cell. Other approaches include the count of impinging particles on the lower boundary of the domain (Wilson, 1995). In general, statistical ensembles of trajectories provide a better description of the transport processes than a single particle approach. The method follows four basic steps to obtain the SRR. An inversion method, such as Bayesian constraints is in turn applied to obtain flux estimates.

2.1 SRR calculation

2.1.1 (A) Measurements

Available measurements were organized in daily data subsets (blocks). Every daily data block was associated with a set of receptors. Receptors were used as initial points for backward Lagrangian trajectories calculated with the LPDM FLEXPART. Only one run was executed per day, with all ensembles within a day included in the same initial file. Ancillary data allowed us to group trajectories for a posteriori plotting and analysis.

2.1.2 (B) Space time partition

Given a set of available measurements, the period and region of interest for the flux inversion, the partition of the space and the time step resolution for the inversion were selected. The output was a set of vectors of length m describing the spatio-temporal discretization of the sources. A subsequent step interpolates a priori fluxes from different inventories into the space-time grid.

The sources were subdivided in a rectangular grid of $0.1^{\circ} \times 0.1^{\circ}$ containing the TBA. An adaptive aggregation was performed to separate the far field (the WRF domain covering East Asia) from the near field (the TBA). A total of 227 subsets of aggregated grid cells was used for every time step. Source geometry specifications allowed us to interpolate corresponding a priori fossil and biogenic flux and boundary/background conditions. As one of the objectives was to assess the impact of a priori information

ACPD
12, 10623–10649, 2012

from different inventories, we used as a priori constraints EDGAR and CDIAC fluxes. The time step of the retrieved sources varied between 1 and 12 h during the period of interest with a default time step of 3 h. Given that emissions 3 days prior to measurement are unlikely to affect receptor, the period of interest has been defined as 72 h prior to measurement for every measurement point. Although background concentrations may be affected by sources outside the chosen domain due to the strength of the source under study, sensitivity tests indicate that they represent a small fraction of the CO_2 measured. Hence, the background value is chosen to match an open ocean site (Mauna Loa taken from NOAA/ESRL, Conway et al., 1988). Nevertheless, this can be changed if background concentrations are provided by a global model with reduced uncertainty. In contexts where the transport and initial conditions are provided with sufficient accuracy, even small scale features of the data time series such as peaks and gradients can be reconstructed with the model (Pisso and Legras, 2008).

2.1.3 (C) Trajectory calculations for mesoscale Lagrangian inversions

Trajectories were calculated with a modified version of the LPDM FLEXPART (Stohl et al., 2005). Different meteorological wind fields were used, including ECMWF ERA interim (EI) and WRF, that can be used to assess transport uncertainty. The trajectory calculations followed for the approach outlined in Pisso et al. (2010). Combined with gridded representations of emissions and concentrations, they allow calculation of Lagrangian reconstructions.

2.1.4 (D) source-receptor relationship (SRR) calculation

This section describes how to calculate the source receptor relationship (SRR) and set other parameters such as PBL the model.

ACPD
12, 10623–10649, 2012

The mixing ratio $\chi(x,t)$ of an atmospheric tracer can be inferred from the previous distribution and sources by the (continuous) Green's function of the diffusion equation $\mathcal{G}$:

$$\chi(x,t) = \int_y \mathcal{G}(x,t;y,s)\chi(y,s)dy + \int_0^t\int_y \mathcal{G}(x,t;y,s)\dot{\chi}(y,s)dyds + \int_0^t\int_S \mathcal{G}\nabla\chi - \chi\nabla\mathcal{G}dSds$$

where χ represents a mixing ratio (in this context the background), $\dot{\chi}$ represents a bulk volume source (in this context the anthropogenic CO_2 emissions) and the kernel $\mathcal{G}$ represents a continuous point-wise probability transition (atmospheric transport and mixing processes). Surface density emission fluxes are formally described by the third term in the equation, however because of numerical limitations this information is usually included in the second term, using some representation of the PBL and diluting the emissions in the 3-D lower grids of the domain.

$\mathcal{G}$ allows to perform 4 dimensional tracer reconstructions (provided $t > s$) and can be numerically estimated from backward trajectory calculations with a discretized G. The trajectories include information from sub-grid scale turbulence modeled as a stochastic processes. Histograms of backward trajectories provide estimates of the transition probability function G or more generally the master equation.

The basic output is a matrix **M** (the SRR), the selected CO_2 data and the emission regions that are compatible with the matrix **M**.

The main component of the output at this step is the Jacobian matrix, i.e. the linearization of the transport operator. This matrix of dimensions (number of observations) × (number of flux regions × time steps) is essentially a histogram of particles within the PBL over the emission regions. The number of rows of the matrix matches the number of receptors, and hence a vector of CO_2 values is stored alongside the matrix. Another vector of the same size is required to store the background values with respect to which concentration perturbation is to be calculated. Several sources of data for the background have been used for testing purposes including a range of

ACPD
12, 10623–10649, 2012

fixed values during short periods, direct interpolation from the output of global (ACTM) and regional (WRF-chem) models, and diffusive Lagrangian reconstructions based on the same models. Due to the inherent uncertainty associated with these estimates, we have chosen to use averages of measurements (with the Mauna Loa time series as the default value). The columns of the matrix correspond to the emission regions considered to have a non-negligible impact on the measured data available for inversion. We are considering a time dependent set of sources covering the TBA. The default setting is a grid of 0.1° in the intervals [132° N 144° N 31° E 40° E]. One of the advantages of using a Lagrangian methodology is that as the grid is used for post processing of the trajectory calculations, the space partition setting is flexible for sensitivity studies. As grids far away from the source have less impact on the measurements, the size of the region increases with distance from the measurements. The code accepts any partition in regions of this grid. It is also possible to aggregate regions after the calculation, although the increase of the resolution requires more computational time.

Numerically, the SRR can be estimated using the residence time of an ensemble of trajectories in a designated volume of space.

The sensitivity of the mass mixing ratio of CO_2 at the receptor to a mass emission at the source can be expressed as the mean time spent within a volume source for those trajectories visiting the source of interest, divided by the air density and the height of the volume source (associated with the PBL). It requires a (simplified) PBL representation (Wilson and Sawford, 1996; Seibert and Frank, 2004) to convert surface mass fluxes into volume mixing ratios:

$$\frac{\partial \chi_{CO_2}}{\partial F} = \frac{1}{N} \sum_{n=1}^{N} \frac{\Delta t_n}{\rho_{air} d}$$

where ρ_{air} is the air density, Δt_n the time step, d the thickness of the footprint layer (layer within the PBL where trajectories are counted) and n the index of the N trajectories arriving at a certain receptor. It has been argued (Seibert and Frank, 2004) that

ACPD
12, 10623–10649, 2012

provided that the footprint layer lies within a well mixed PBL, the source receptor relationship is independent of d (Seibert, 2004; Lin, 2003). The customary value of d is to the order of 300 m.

2.2 Bayesian inversion

The previous section described the calculation of the SRR based on trajectories. The inversion is performed using the measurements, the background and the bottom up estimations interpolated in (B), used as a priori emissions for Bayesian inversion. We have chosen to apply a Least Squares Bayesian inversion method to the resulting SRR based on a technique previously used in the literature (Menke, 1984; Tarantola, 2005) adapted to the present case.

M is available for all measurements y, the different a priori inventory data S_0 and all winter months from 2005 to 2009. For every month, a local sub matrix with the rows corresponding to each day and the columns corresponding to the significant emission regions was constructed.

For every day, there is a daily matrix **M** and a daily set of measurements and sources. The geometry of the sources matching these measurements and transport operator **M** were selected from the vector of sources defined previously for the whole period of inversion.

The information gathered in the previous section yields the basic input required for Bayesian inversion: the matrix for the linearized transport operator **M**, the vector of constraining measurements y (perturbations respect to the background concentration) and the a priori fluxes S_0.

$$S = S_0 + C_S \mathbf{M}^{\mathrm{T}} \left(\mathbf{M} C_D \mathbf{M}^{\mathrm{T}} + C_D \right)^{-1} (y - \mathbf{M} S_0)$$

Where S is the a posteriori flux, C_S is the covariance of the fluxes, C_D the covariance of the measurements (Tarantola, 2005).

ACPD
12, 10623–10649, 2012

Different backgrounds were used to test the sensitivity of the method, although arguably the most reasonable background would be from a clean air site such as Yonagunishima, Minamitorishima or Mauna Loa. The interpolated values for the a priori fluxes are based on the inventories to be tested and must comply with the format established for that day. The covariance matrices C_D and C_F are determined based on the a priori uncertainties. Two scenarios were chosen for testing uncertainty: the standard identity functions and a 200 % variance (Gurney et al., 2002).

3 Data

3.1 Measurements

We have integrated CO_2 data from ground stations, a tall tower and in-situ aircraft measurements covering the Tokyo Bay Area (Fig. 1).

In situ high resolution measurements being used include

(i) Tsukuba tall tower (measurement of CO_2 in the sampled air from inlets located at 25, 100, and 200 m introduced by the diaphragm pump to the NDIR in the experimental field building) for 2007 (Inoue and Matsueda, 1996, 2001). The concentration of CO_2 is calculated based on the MRI87 scale (Inoue and Matsueda, 1996). The difference in CO_2 concentration scale between WMO mole-fraction and MRI87 is less than 0.2 ppm for the ambient CO_2 level, although it depends on the mixing ratios (Ishii et al., 2004).

(ii) Aircraft CO_2 measurements are taken from the Continuous CO_2 Measuring Equipment (CME) on board a Japan Airlines (JAL) passenger aircraft by the Comprehensive Observation Network for TRace gases by AIrLiner (CONTRAIL) project (Machida et al., 2008). Continuous CO_2 measurement over the Narita airport are used in this study during the ascending and descending of the aircraft.

ACPD
12, 10623–10649, 2012

The measurements are reported in NIES-95 standard scale. Data covers 2007 to 2009.

(iii) Atmospheric CO_2 hourly concentration data, Mt. Dodaira and Kisai, World Data Cent. for Greenhouse Gases (WDCGG), Japan Meteorol. Agency, Tokyo. (Available at http://gaw.kishou.go.jp/wdcgg.html.) The absolute scales of these measurements are WMO mole fraction scale. We have chosen data from 2005 to 2009 for this analysis.

3.2 Initial conditions, boundary conditions and a priori information

The a priori information is drawn from different inventory data: EDGAR version 4 and CDIAC. It is worth to stress that in the Tokyo Bay Area, the biogenic fluxes then represent just a small fraction of the anthropogenic emissions and hence their impact on the final inversion result is modest. A large source of uncertainty is the background CO_2 value. We have tested different options, including model output from AGCM and WRF. A conservative but robust estimate are the measurements from the clear air oceanic sites such as Mauna Loa observatory and Yonaguni island.

3.3 Models

We have used two global scale trajectory codes: FLEXPART 8.1 (Stohl et al., 2005) and TRACZILLA (Legras et al., 2005; Pisso et al., 2010) driven by ERA Interim (EI) winds (Simmons et al., 2007). Regional scale modelling was performed using FLEXPART-WRF (de Foy et al., 2009) driven by WRF – CO_2 winds For our simulation, WRF-CO_2 was configured with 27 km grid spacing domain over East Asia. We choose Lambert Conformal map projection for the model domain with 165 × 132 grid cells (Grell et al., 2005; Takigawa et al., 2007; Ballav et al., 2012). The domain is centered at (35° N, 133° E), which is near Tokyo. The model has 30 vertical layers up to 100 hPa, and 11 layers are located within 2 km above the ground level. Different meteorological advection fields have been used in this study related to different Lagrangian models.

ACPD
12, 10623–10649, 2012

TRACZILLA and FLEXPART 8.1 are driven by ERA Interim (EI) reanalysis. ERA-Interim is the latest ECMWF reanalysis with a spectral truncation of T255L. Global coverage 3 h intervals and 1° × 1° spatial resolution were used for these analyzed winds.

4 Results

We have selected a set of measurements for analysis: the winter months for the years 2005 to 2009. Figure 1 shows the spatial distribution of data used within the region to be assessed for inversion. CONTRAIL and WDCGG data spanned from 2005 to 2009. The sites of WDCGG provide a continuous record of data. Tsukuba tall tower data was used for 2007. The total amount of data points used in this work is 176 414. The trajectories have been calculated for all available receptors with ERA Interim and WRF winds. One run per day was performed starting on every receptor measurement point for an ensemble of 100 trajectories. The particle output was stored every hour for post processing for a period of 7 days. Nevertheless, only the first 3 days are significant for TBA flux estimation.

4.1 Calculation of SRR

For the period under consideration (2005 to 2009), ensembles of trajectories associated with the measurements were processed to estimate the SRR for all measurement points. The fluxes were retrieved at 3 h time resolution. The results are based on a 20 km × 20 km grid which can be aggregated in different ways (e.g. the prefecture boundaries of the Kanto area). Minimal dimensions of the daily configuration were 48 × 2724 for days containing only WDCGG sites data. As the columns outnumber the rows, the system required regularization for matrix inversion.

The matrix is solved on a daily basis. Besides allowing a faster calculation than the full matrix, the day by day calculation set out a simple parallelization methodology. For

ACPD
12, 10623–10649, 2012

each day of measurements the algorithm provides an estimate of fluxes for the previous three days. The results are averaged monthly to reduce random variability.

Figure 2 shows an example of the SRR matrix corresponding to the 1st of January 2007. This figure demonstrates a decreasing influence of the emission regions as time evolves backwards. After 3 days the influence of the source regions is negligible and hence it was not taken into account. The influence of far field sources is reduced by mixing, and given the strength of the Tokyo sources it can be overlooked at an initial stage. Patterns calculated with ERA Interim and WRF winds show a considerable agreement. In general, the shapes of the clouds of points used to construct these matrices show a consistent picture of transport. As for the absolute values, the L^1 norm (the sum of the absolute values) of the difference is to the order of 10 % of either matrix WRF or ERA Interim. This is significant because both model's meteorologies are based on different assimilation systems (ECMWF and NCEP). The fact that they show a consistent picture provides necessary grounds for any subsequent analysis. Without agreement between different transport models, further conclusions may be compromised.

4.2 Flux inversion

Given a certain degree of confidence in the description of the transport, an inversion-based constrain on the fluxes can be attempted. Several factors have an impact on the inversion results including the a priori fluxes, background and measurement selection. In Fig. 3, CO_2 fluxes from fossil fuel burning are shown. The first column shows the EDGAR and CDIAC inventories in the TBA. The second, third and fourth columns correspond to 2005, 2007 and 2009 retrieved fluxes respectively. The upper row shows the geographical distribution of a posteriori fluxes using EDGAR as a priori. The lower row shows the geographical distribution of a posteriori fluxes using CDIAC as a priori.

The geographical distribution of the fluxes in the TBA illustrates how the a priori information introduced by EDGAR regularizes the inversion, providing a picture consistent with third party information. Error reduction is obtained in the grid cells closer to the measurement data, such as Kisai, Dodaira, Tsukuba and Narita. The estimates show

ACPD
12, 10623–10649, 2012

a weak variability over time, in agreement with previously reported regional inventory data in Japan. In the case of CDIAC (lower row), the a priori grid is much coarser, but it can be used as an interesting benchmark for the method. For example, the inversion adds spatial information, as can be seen in panels f, g and d. The spatial distribution of emissions with CDIAC a priori has much less contrast compared to EDGAR 4. These modifications are likely to be higher in those regions and during periods in which more information was available from measurements.

Figure 4 shows the impact of CONTRAIL data on the geometry of retrieved fluxes. The upper left panel shows the result of the inversion using all available data including WDCGG stations, the Tsukuba tall tower and CONTRAIL. The upper right panel shows the result of the inversions including only WDCGG stations and Tsukuba data. The lower left panel displays the a priori used, EDGAR 4 for 2005 for comparison. The geometry of the retrieved fluxes is consistent with the inventory data. The difference is larger in those grids with higher flux value such as the center of Tokyo and in the grids containing the largest power plants. The lower right panel shows the difference between the results using all data with respect to the results based on WDCGG sites only. In the most urbanized region of Tokyo the difference is up to 21 % higher using all data measurements. This illustrates to what extent the availability of data has a large impact on flux inversion results.

The calculation of a longer time series of inversions provides information about the time evolution of fluxes, their variability and trends. In order to study the time evolution of fluxes we have calculated the monthly average of daily inversions for the available period of data from 2005 to 2009. Figure 5 shows a set of time series of averaged a posteriori fluxes. The fluxes were calculated for the winter months, from December to March in order to avoid uncertainties associated with summer biogenic activity and variable mixing within the PBL. Different data sets were created for both CDIAC and EDGAR a priori fluxes. In both cases, the retrieved fluxes were higher than the a priori. The Bayesian inversion suggested that the inventories underestimated the fluxes required to match measurements. In order to determine to what extent this behavior

ACPD
12, 10623–10649, 2012

depended on the magnitude of the a priori fluxes, we calculated the inversions increasing the a priori fluxes by a factor of 2 and 3. It was found that a factor of 2 slightly overestimated the fluxes and a factor of 3 largely overestimates the fluxes. The fact that the equilibrium point is slightly below 2 times the EDGAR values means that the system is able to confirm that CDIAC underestimates the fluxes. In the present case this was expected and it is due mainly to the coarse resolution of the CDIAC inventory. In the case of TBA CO_2 emissions an error threshold of 5–10 % would be required for short timescale variability assessment. Such thresholds are still beyond the capabilities of the current methodology given the data availability and the transport/mixing model uncertainties. In particular the region still remains under-constrained given the sparse observation network. Because of the uncertainties related to the transport model, it cannot be unequivocally asserted that EDGAR underestimates Tokyo emissions. Nevertheless a reduction of the uncertainty below the threshold of 100 % represents an improvement respect to regional inversions performed with global models (Gurney et al., 2002).

The time series of retrieved fluxes allowed us to carry out a trend analysis. The CO_2 fluxes in the TBA have shown a slow increase in the first decade of the 21st century. The evolution of fluxes over time presents a flat trend that is compatible with the a priori information provided by the inventories (http://www.kankyo.metro.tokyo.jp/en/data/). This static trend could be explained by several factors including negative population growth in Japan, the increase in efficiency in energy use and the roll out of CO_2 mitigation policies.

5 Discussion

The flux values obtained are consistent with the values of Moriwaki and Kanda (2004) to the order of $2.5 \times 10^{-7}\,kg_{CO_2}\,m^{-2}\,s^{-1}$ based on direct micrometeorological measurements. The average flux values obtained in this study are lower than those of Moriwaki and Kanda (2004). This may be due to the fact that a larger area encompassing rural

ACPD
12, 10623–10649, 2012

areas of Kanto is selected in our average, whereas Moriwaki and Kanda (2004) focused on a restricted suburban area. In addition, our estimates are strongly affected by the a priori baseline, e.g., EDGAR may underestimate the actual flux. The values are also consistent with the yearly average value of 1.9124×10^{-7} obtained by Kordowski and Kuttler (2010). They study a park area in Essen, Germany, which is somewhat consistent with our mixed urban/rural area in the TBA. In such areas, while some biogenic uptake occurs it is not expected to overtake anthropogenic emissions, warranting a positive flux throughout the year. It is worth bearing in mind that these comparisons are being made between pointwise measurements and a large area inversion.

Several sources of uncertainties affect the inversion process, namely data, model representation and errors in the estimation of the a priori fluxes. Additional sources of error include the impact of the PBL parametrization. The construction of the SRR involves the translation of 2-D flux densities to 3-D mixing ratio or concentrations. The Green's function method is best suited to represent probability transitions between regions of the same dimension (i.e., 3-D to 3-D). Although a rigorous formulation exists for the consideration of boundary fluxes for mixed Neumann-Dirichlet boundary conditions (Morse and Feshbach, 1953; Holzer and Hall, 2000), it is not well suited for numerical computations. This is because such a formulation requires the calculation of the Green's function gradient at the boundary of the domain, which can result in a large source of error. Instead, an additional step is often performed for the parameterization of the mixing within PBL. In this study we have used a PBL height consistent with the 3-D transport model used for advection (ERA Interim or WRF). The use of measurements to constrain PBL height is limited by the spatial distribution required within the inversion area.

Given the small scale resolution required for city size flux estimations, spatial an time resolution can be a source of error. The compliance with a CFL condition is required. Typical wind speed is to the order of $20\,\mathrm{km\,h^{-1}}$. The resolution of the horizontal grid is 20 km and the time step of the output of trajectories is 1 h. The transport timescale between the sites of Kisai or Narita and the center of Tokyo is of the order of one hour.

ACPD
12, 10623–10649, 2012

The selection of measurement points can also contribute to uncertainty, as seen in Fig. 5 for the year 2007 when the availability of more measurement points provided higher sensitivity for the inversions. Furthermore Fig. 5 illustrates the large impact of the selection of the a priori flux estimate on the inverted flux values. Fluxes estimated with different inventories (Fig. 5) suggest that in both EDGAR and CDIAC inventories underestimate the actual emissions. This exercise is useful to distinguish the performance of EDGAR and CDIAC and suggests a method for the selection of the most appropriate inventory. For the purposes of this study, the optimal a priori inventory was EDGAR. A hypothetical exercise doubling the value of EDGAR a priori emissions yields estimates that are lower than the a priori. Doubling the emissions results in excessive values that must then be lowered by the inversion to fit the measurements. In this case it is apparent that the underestimation is due to the coarser resolution of CDIAC inventory. Nevertheless, this method could be applied to finer resolution a priori fluxes although it is likely that more CO_2 data, over a larger, denser geographical distribution would be necessary in order to further reduce uncertainty. Nevertheless, should the present methodology be further refined to reduce uncertainty, it may eventually be applicable as a policy tool. More sophisticated techniques such as observation targeting and optimal network design may be applicable. It can be argued that the availability and accuracy of TBA inventory data makes it a suitable area for benchmark model inversion methodologies.

Other studies applied the Lagrangian inversion technique to other greenhouse gases such as CFCs. Keller et al. (2011) estimated under reported emissions of HFC-23 using a method previously presented by Stohl et al. (2010). They used the standard input procedure for FLEXPART adapted to data from the Jungfraujoch station. In this study a different initialization procedure was used allowing us to include aircraft data at full resolution: all 4-D information for every aircraft measurement point is used as in Pisso et al. (2010).

Interestingly, at first sight it appears that that the relatively large availability of in situ data yields the ability to explore new problems associated with overdetermined sys-

ACPD
12, 10623–10649, 2012

tems, as opposed to underdetermined systems characteristic of global inversions. In fact, the present case can be treated as an overdetermined system provided average fluxes are treated and some assumptions regarding the representativity of the measurements are made. However, owing to the high resolution of in situ aircraft data, a large number of data are highly correlated and do not convey independent information. A solution to this problem would require the collection of data in locations that optimally reduce error. This concept has been explored in the fields of data assimilation and network design (Patra and Maksyutov , 2002).

6 Conclusions and outlook

In this study, we have applied a Bayesian inversion technique combining Lagrangian particle dispersion model in backward mode with a composite of CO_2 measurements including ground sites, tall tower and aircraft data. We have found that the better constraints on the spatial distributions are obtained using all data including CONTRAIL aircraft data with respect to inversions calculated using ground sites only. Such improved description of the spatial structure is noticeable even for coarse a priori fluxes intended for global models, such as the CDIAC inventory. When longer time series of spatially averaged fluxes were calculated, we found little evidence of trends in TBA CO_2 fluxes, in agreement with local inventory estimation based on third party information. The reliability of these estimates is subject to uncertainties in the transport models. Additional work is required to improve planetary boundary layer parametrizations and other precesses of regional transport. We have found that the amount of input measurement data has a large impact on the results of the inversions. Differences in inverted fluxes in Central Tokyo amounted to up to 21 % adding aircraft data from the CONTRAIL dataset. An improvement in the coverage and density of the network distribution is expected to significantly contribute to the overall quality of the inversions. The method may provide an appropriate tool for selecting a priori flux inventories on

ACPD
12, 10623–10649, 2012

the condition that sufficient data are collected in adequate locations. Further reduction in uncertainty is required in order to establish a method suitable to inform policy.

References

BallavS., Patra, P. K., Takigawa, M., Ghosh, S., De, U. K., Murayama, S., Mukai, H., Hashimoto, S.: Simulation of CO_2 concentration over east asia using regional transport model WRF-CO_2, in revision, J. Meteorol. Soc. Jpn., 2012. 10633

Conway, T., Tans, P., Waterman, L., Thoning, K., Masarie, K., and Gammon, R.: Atmospheric carbon dioxide measurements in the remote global troposphere, Tellus, 40B, 81–115, 1988. 10628

de Foy, B., Zavala, M., Bei, N., and Molina, L. T.: Evaluation of WRF mesoscale simulations and particle trajectory analysis for the MILAGRO field campaign, Atmos. Chem. Phys., 9, 4419–4438, doi:10.5194/acp-9-4419-2009, 2009. 10626, 10633

Enting, I. G.: Inverse Problems in Atmospheric Constituent Transport, Cambridge Univ. Press, Cambridge, UK, 392 pp., 2002. 10625

European Comission: Emission Database for Global Atmospheric Research (EDGAR), release version 4.0., available at: http://edgar.jrc.ec.europa.eu/faq.php, last access: 10 December 2009, 2009. 10624

Grell, G. A., Peckham, S. E., Schmitz, R., McKeen, S. A., Frost, G., Skamarock, W. C., and Eder, B.: Fully coupled "online" chemistry within the WRF model, Atmos. Environ., 39, 6957–6975, 2005. 10633

Gurney, K. R., Law, R. M., Denning, A. S., Rayner, P. J., Baker, D., Bousquet, P., Bruhwiler, L., Chen, Y.-H., Ciais, P., Fan, S., Fung, I. Y., Gloor, M., Heimann, M., Higuchi, K., John, J., Maki, T., Maksyutov, S., Masarie, K., Peylin, P., Prather, M., Pak, B. C., Randerson, J., Sarmiento, J., Taguchi, S., Takahashi, T., and Yuen, C.-W.: Towards robust regional estimates of CO_2 sources and sinks using atmospheric transport models, Nature, 415, 626–630, doi:10.1038/415626a, 2002. 10625, 10632, 10637

Holzer, M. and Hall, T.: Transit-time and tracer-age distributions in geophysical flows, J. Atmos. Sci., 57, 3539–3558, doi:10.1175/1520-0469(2000)057<3539:TTATAD>2.0.CO;2, 2000. 10638

ACPD
12, 10623–10649, 2012

Inoue, H. Y. and Matsueda, H.: Variations in atmospheric CO_2 at the Meteorological Research Institute, Tsukuba, Japan, J. Atmos. Chem., 23, 137–161, 1996. 10632

Inoue, H. Y. and Matsueda, H.: Measurements of atmospheric CO_2 from a meteorological tower in Tsukuba, Japan, Tellus B, 53, 205–219, 2001. 10632

Ishii, M., Saito, S., Tokieda, T., Kawano, T., Matsumoto, K., and Yoshikawa-Inoue, H.: Variability of surface layer CO_2 parameters in the Western and Central Equatorial Pacific, Global Environ. Changes Ocean Land B, 53, 59–94, 2004. 10632

Keller, C. A., Brunner, D., Henne, S., Vollmer, M. K., O'Doherty, S., and Reimann, S.: Evidence for under-reported Western European emissions of the potent greenhouse gas HFC-23, Geophys. Res. Lett., 38, L15808, doi:10.1029/2011GL047976, 2011. 10639

Kordowski, K. and Kuttler, W.: Carbon dioxide fluxes over an urban park area, Atmos. Environ., 44, 2722, 2010. 10638

Lauvaux, T., Pannekoucke, O., Sarrat, C., Chevallier, F., Ciais, P., Noilhan, J., and Rayner, P. J.: Structure of the transport uncertainty in mesoscale inversions of CO_2 sources and sinks using ensemble model simulations, Biogeosciences, 6, 1089–1102, doi:10.5194/bg-6-1089-2009, 2009. 10625

Legras, B., Pisso, I., Berthet, G., and Lefèvre, F.: Variability of the Lagrangian turbulent diffusion in the lower stratosphere, Atmos. Chem. Phys., 5, 1605–1622, doi:10.5194/acp-5-1605-2005, 2005. 10633

Lin, J. C., Gerbig, C., Wofsy, S. C., Chow, V. Y., Gottlieb, E., Daube, B. C., and Matross, D. M.: Designing Lagrangian experiments to measure regional-scale trace gas fluxes, J. Geophys. Res., 112, D13312, doi:10.1029/2006JD008077, 2007. 10625

Machida, T., Matsueda, H., Sawa, Y., Nakagawa, Y., Hirotani, K., Kondo, N., Goto, K., Ishikawa, K., Nakazawa, T., and Ogawa, T.: Worldwide measurements of atmospheric CO_2 and other trace gas species using commercial airlines, J. Atmos. Oceanic. Technol., 25(10), 1744–1754, 2008. 10632

Menke, W.: Geophysical Data Analysis: Discrete Inverse Theory, Academic Press, San Diego, USA, 285 pp., 1984. 10631

Moriwaki, R. and Kanda, M.: Seasonal and diurnal fluxes of radiation, heat, water vapor, and carbon dioxide over a suburban area, J. Appl. Meteorol., 43, 1700–1710, 2004. 10625, 10637, 10638

Morse, P. M. and Feshbach, H.: Methods of theoretical physics, Part I, McGraw-Hill, New York, 857–859, 1953. 10638

ACPD

12, 10623–10649, 2012

Patra, P. K. and Maksyutov, S.: Incremental approach to the optimal network design for CO_2 surface source inversion, Geophys. Res. Lett., 29, 1459, doi:10.1029/2001GL013943, 2002. 10640

Patra, P. K., Law, R. M., Peters, W., Rödenbeck, C., Takigawa, M., Aulagnier, C., Baker, I., Bergmann, D. J., Bousquet, P., Brandt, J., Bruhwiler, L., Cameron-Smith, P. J., Christensen, J. H., Delage, F., Denning, A. S., Fan, S., Geels, C., Houweling, S., Imasu, R., Karstens, U., Kawa, S. R., Kleist, J., Krol, M. C., Lin, S.-J., Lokupitiya, R., Maki, T., Maksyutov, S., Niwa, Y., Onishi, R., Parazoo, N., Pieterse, G., Rivier, L., Satoh, M., Serrar, S., Taguchi, S., Vautard, R., Vermeulen, A. T., and Zhu, Z.: TransCom model simulations of hourly atmospheric CO_2: Analysis of synoptic-scale variations for the period 2002–2003, Global Biogeochem. Cy., 22, GB4013, doi:10.1029/2007GB003081, 2008. 10625

Pisso, I. and Legras, B.: Turbulent vertical diffusivity in the sub-tropical stratosphere, Atmos. Chem. Phys., 8, 697–707, doi:10.5194/acp-8-697-2008, 2008. 10628

Pisso, I., Real, E., Law, K. S., Legras, B., Bousserez, N., Attié, J. L., and Schlager, H.: Estimation of mixing in the troposphere from Lagrangian trace gas reconstructions during long range pollution plume transport, J. Geophys. Res., 114, D19301, doi:10.1029/2008JD011289, 2010. 10626, 10628, 10633, 10639

Risken, H.: The Fokker-Planck Equation: Methods of Solutions and Applications, Springer Series in Synergetics, Berlin, Germany, 472 pp., 1989. 10626

Seibert, P. and Frank, A.: Source-receptor matrix calculation with a Lagrangian particle dispersion model in backward mode, Atmos. Chem. Phys., 4, 51–63, doi:10.5194/acp-4-51-2004, 2004. 10626, 10630

Simmons, A., Uppala, S., Dee, D., and Kobayashi, S.: ERA-Interim: new ECMWF reanalysis products from 1989 onwards, ECMWF Newsl., 110, 29–35, 2007. 10633

Stohl, A., Forster, C., Frank, A., Seibert, P., and Wotawa, G.: Technical note: The Lagrangian particle dispersion model FLEXPART version 6.2, Atmos. Chem. Phys., 5, 2461–2474, doi:10.5194/acp-5-2461-2005, 2005. 10628, 10633

Stohl, A., Kim, J., Li, S., O'Doherty, S., Mühle, J., Salameh, P. K., Saito, T., Vollmer, M. K., Wan, D., Weiss, R. F., Yao, B., Yokouchi, Y., and Zhou, L. X.: Hydrochlorofluorocarbon and hydrofluorocarbon emissions in East Asia determined by inverse modeling, Atmos. Chem. Phys., 10, 3545–3560, doi:10.5194/acp-10-3545-2010, 2010. 10639

ACPD
12, 10623–10649, 2012

Takigawa, M., Niwano, M., Akimoto, H., and Takahashi, M.: Development of a one-way nested global-regional air quality forecasting model, SOLA, 3, 81–84, doi:10.2151/sola.2007?021, 2007. 10633

Tarantola, A.: Inverse problem theory and methods for model parameter estimation, Society for Industrial and Applied Mathematics, Philedelphia, USA, 342 pp., 2005. 10625, 10631

Tolk, L. F., Peters, W., Meesters, A. G. C. A., Groenendijk, M., Vermeulen, A. T., Steeneveld, G. J., and Dolman, A. J.: Modelling regional scale surface fluxes, meteorology and CO_2 mixing ratios for the Cabauw tower in the Netherlands, Biogeosciences, 6, 2265–2280, doi:10.5194/bg-6-2265-2009, 2009. 10625

Wilson, J. D. and Sawford, B. L.: Review of stochastic Lagrangian models for trajectories in the turbulent atmosphere, Bound.-Lay. Meteorol., 78, 191–210, 1996. 10630

ACPD

12, 10623–10649, 2012

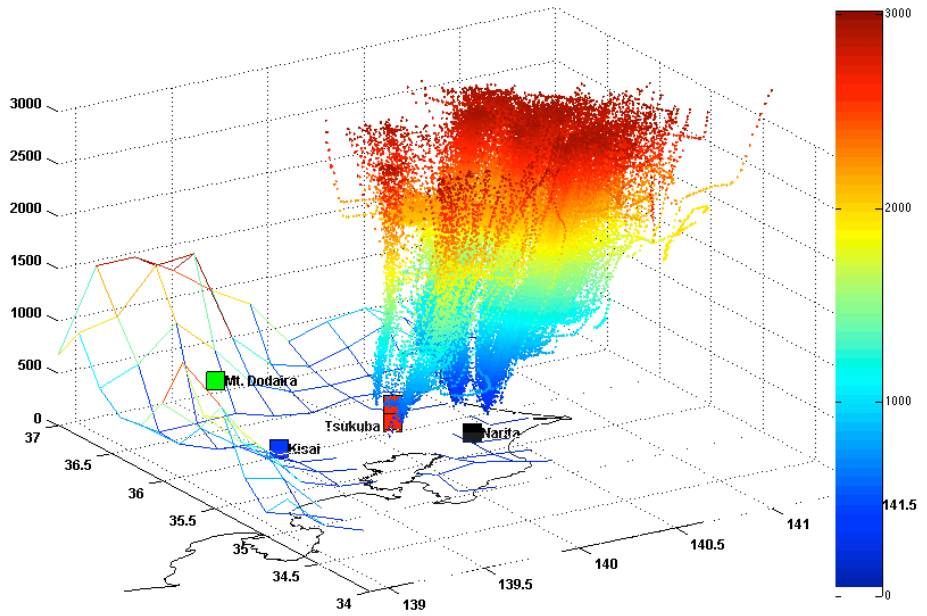

Fig. 1. Sampling location used in this study including geographical distribution of CONTRAIL data. CONTRAIL measurements provide high resolution sampling of the area surrounding Tokyo. The gridded surface indicates topography as resolved by the inversion model.

ACPD
12, 10623–10649, 2012

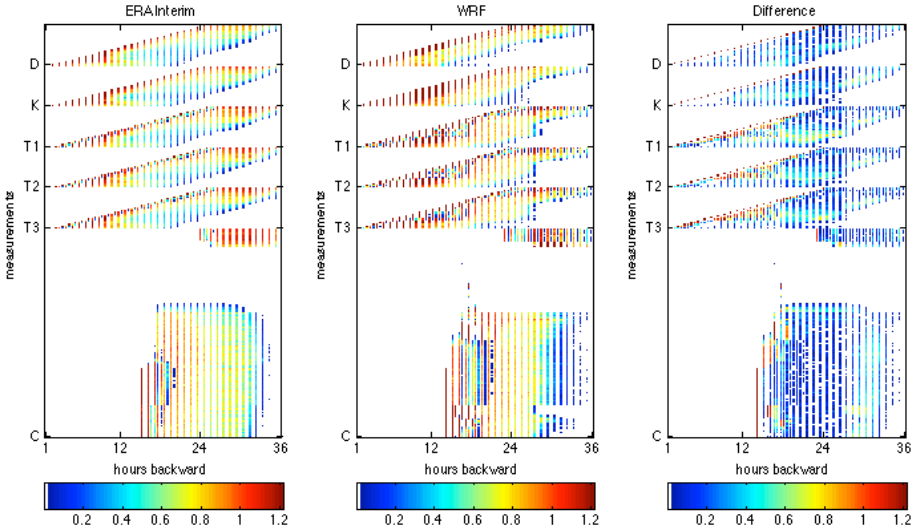

Fig. 2. Source receptor relationship matrix calculated with different winds. Left: panel ERA Interim. Center panel: WRF. Right panel: difference. Vertical axis represents measurements grouped by site and release time (D = Dodaira, K = Kisai, T = Tsukuba, C = CONTRAIL). Horizontal axis represents the Tokyo Bay Area emission sources under consideration hourly between 24:00 JST of the release day and 36 h backward in time. Color scale represents the SRR value in $(kg_{CO_2}\ m^2\ s^{-1})^{-1}$. The integrated difference is of the order of 10 % of the SRR calculated either with WRF of with ERA Interim winds.

ACPD
12, 10623–10649, 2012

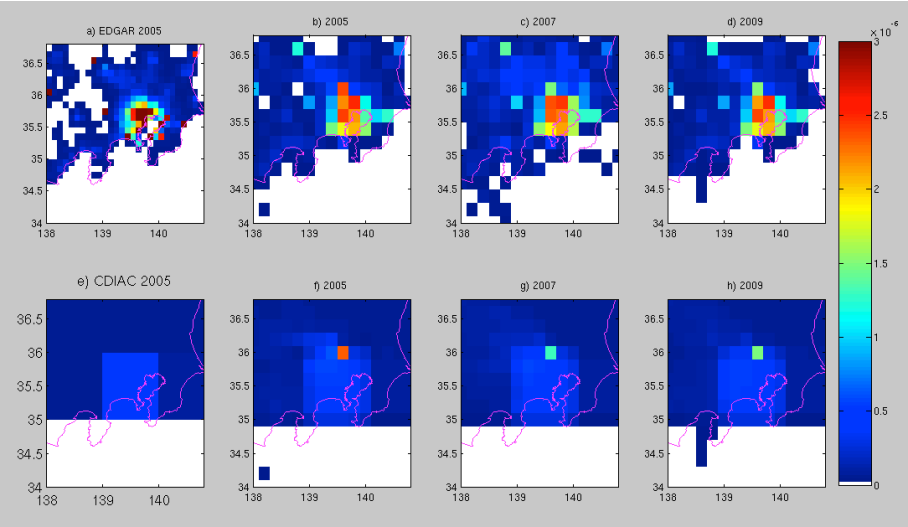

Fig. 3. CO_2 fluxes from fossil fuel burning (in $kg_{CO_2}\,m^2\,s^{-1}$) Left colum: EDGAR and CDIAC a priori fluxes. **(b, f)** Retrieved fluxes using WCDGG data in 2005, 2007 and 2009 with CDIAC and EDGAR inventories as a priori fluxes.

ACPD
12, 10623–10649, 2012

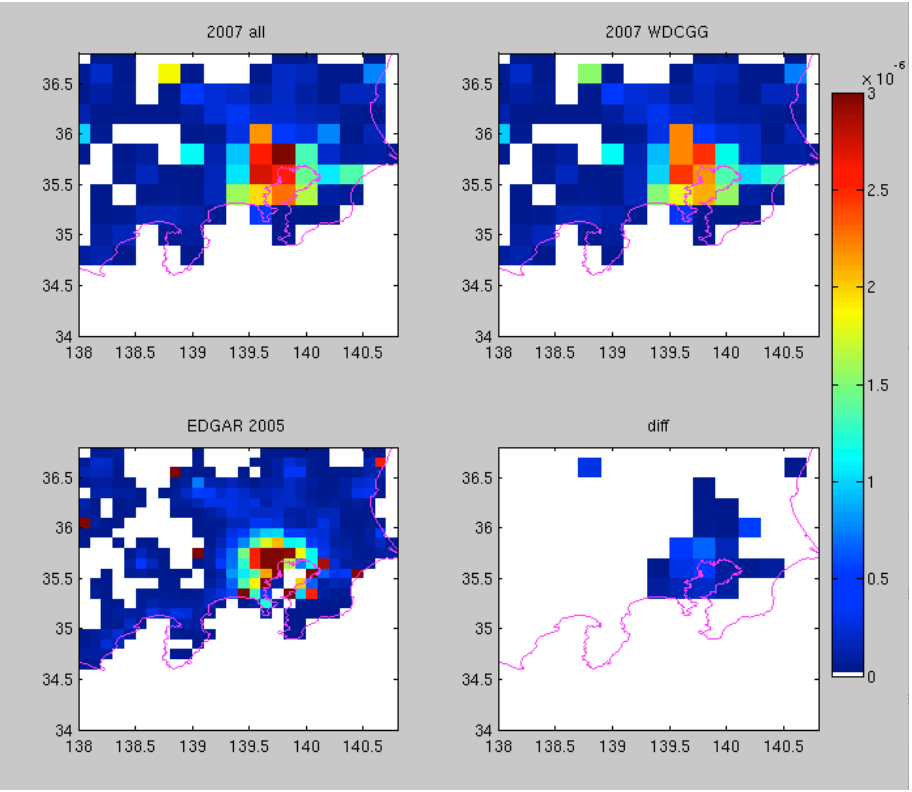

Fig. 4. Impact of CONTRAIL data on the geometry of retrieved fluxes (in $kg_{CO_2}\,m^2\,s^{-1}$). Upper left: fluxes retrieved with all data including CONTRAIL. Upper right: fluxes retrieved with WDCGG and Tsukuba data only. Lower left panel: a priori EDGAR fluxes. Lower right panel: difference between upper panels.

ACPD
12, 10623–10649, 2012

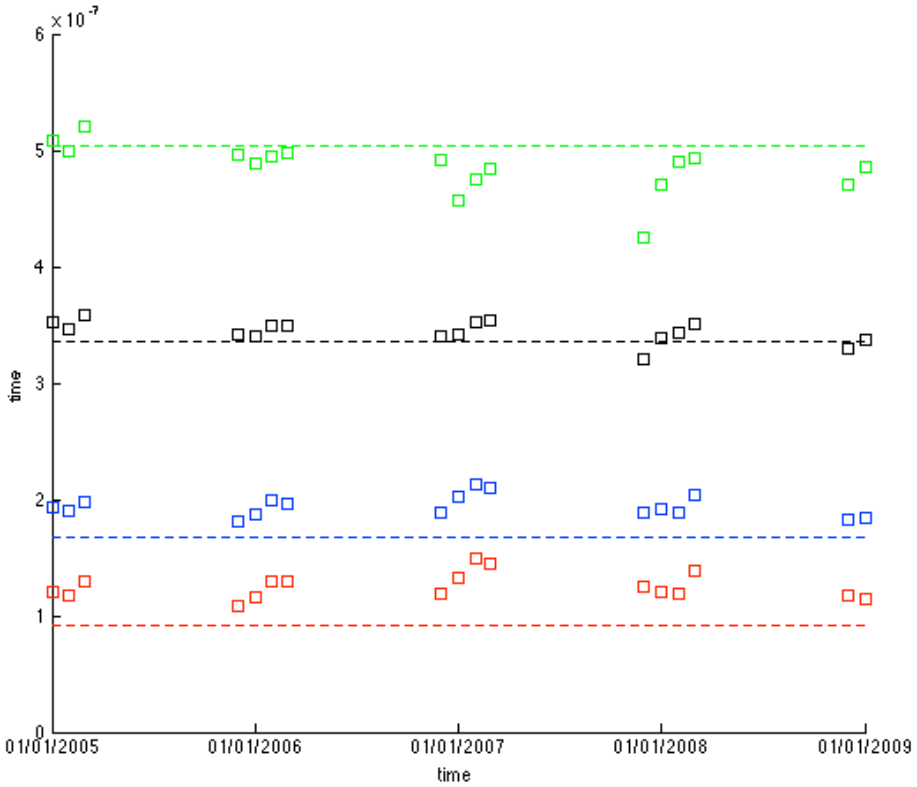

Fig. 5. Time series of spatially and temporally averaged fluxes in $kg_{CO_2}\,m^{-2}\,s^{-1}$. Squares represent monthly Bayesian retrievals (a posteriori fluxes) and dashed lines represent a priori spatial averages. A prioris include: CDIAC (red), EDGAR (blue), 2× EDGAR (black) and 3× EDGAR (green).

ACPD
12, 10623–10649, 2012